Science
AAAS

Memory Metamaterials
T. Driscoll, *et al.*
Science **325**, 1518 (2009);
DOI: 10.1126/science.1176580

Science (print ISSN 0036-8075; online ISSN 1095-9203) is published weekly, except the last week in December, by the American Association for the Advancement of Science, 1200 New York Avenue NW, Washington, DC 20005.

tering becomes more pronounced. Our measurements of the temperature dependence of the mean free path (SOM text S5) show that the conductance oscillation broadens and disappears in the same temperature range ($T \geq 40$ K) where l becomes shorter and transport therefore changes from ballistic to diffusive. This temperature dependence is a further confirmation of theory (*1*).

Two decades ago, Datta and Das proposed an experiment involving spin injection, detection, and spin precession caused by a gate voltage and special relativistic effects on ballistic electrons in a 2DEG. Separate aspects have been demonstrated individually (*3*, *5*, *17*). We have used the nonlocal lateral spin valve geometry to combine these aspects in a single experiment. The InAs single-quantum well used here is an ideal material, because a large spin-orbit interaction modulates a Rashba field by several teslas with a gate voltage range of a few volts.

References and Notes

1. S. Datta, B. Das, *Appl. Phys. Lett.* **56**, 665 (1990).
2. I. Žutić, J. Fabian, S. Das Sarma, *Rev. Mod. Phys.* **76**, 323 (2004).
3. S. A. Crooker *et al.*, *Science* **309**, 2191 (2005).
4. I. Appelbaum, B. Huang, D. J. Monsma, *Nature* **447**, 295 (2007).
5. X. Lou *et al.*, *Nat. Phys.* **3**, 197 (2007).
6. H. C. Koo *et al.*, *Appl. Phys. Lett.* **90**, 022101 (2007).
7. M. Johnson, *Science* **260**, 320 (1993).
8. M. Johnson, R. H. Silsbee, *Phys. Rev. Lett.* **55**, 1790 (1985).
9. F. J. Jedema, H. B. Heersche, A. T. Filip, J. J. A. Baselmans, B. J. van Wees, *Nature* **416**, 713 (2002).
10. Y. Ji, A. Hoffmann, J. S. Jiang, S. D. Bader, *Appl. Phys. Lett.* **85**, 6218 (2004).
11. T. Kimura, J. Hamrle, Y. Otani, K. Tsukagoshi, A. Aoyagi, *Appl. Phys. Lett.* **85**, 3501 (2004).
12. M. Johnson, R. H. Silsbee, *Phys. Rev. B* **76**, 153107 (2007).
13. Yu. A. Bychkov, E. I. Rashba, *JETP Lett.* **39**, 78 (1984).
14. A. Janossy, P. Monod, *Phys. Rev. Lett.* **37**, 612 (1976).
15. Materials and methods are available as supporting material on *Science* Online.
16. J. Nitta, A. Tatsushi, H. Takayanagi, T. Enoki, *Physica E* **2**, 527 (1998).
17. J. Nitta, T. Akazaki, H. Takayanagi, T. Enoki, *Phys. Rev. Lett.* **78**, 1335 (1997).
18. I. Lo *et al.*, *Phys. Rev. B* **65**, 161306(R) (2002).
19. T. H. Sander, S. N. Holmes, J. J. Harris, D. K. Maude, J. C. Portal, *Phys. Rev. B* **58**, 13856 (1998).
20. A. C. H. Rowe, J. Nehls, R. A. Stradling, R. S. Ferguson, *Phys. Rev. B* **63**, 201307 (2001).
21. V. Ya. Aleshkin *et al.*, *Semiconductors* **42**, 828 (2008).
22. C.-M. Hu, J. Nitta, A. Jensen, J. B. Hansen, H. Takayanagi, *Phys. Rev. B* **63**, 125333 (2001).
23. M. I. D'yakonov, V. Yu. Kachorovski. *Fiz. Tekh. Poluprodn.* **20**, 178 (1986) [*Sov. Phys. Semicond.* **20**, 110 (1986)].
24. M. I. D'yakonov, V. I. Perel. *Fiz. Tverd. Tela* **13**, 3581 (1971) [*Sov. Phys. Solid State* **13**, 3023 (1972)].

25. This work was supported by the Korea Institute of Science and Technology Institutional Program.

Supporting Online Material

www.sciencemag.org/cgi/content/full/325/5947/1515/DC1
Materials and Methods
SOM Text
Figs. S1 to S5
References

17 March 2009; accepted 28 July 2009
10.1126/science.1173667

Memory Metamaterials

T. Driscoll,[1]* Hyun-Tak Kim,[2] Byung-Gyu Chae,[2] Bong-Jun Kim,[2] Yong-Wook Lee,[2,3] N. Marie Jokerst,[4] S. Palit,[4] D. R. Smith,[4] M. Di Ventra,[1] D. N. Basov[1]

The resonant elements that grant metamaterials their distinct properties have the fundamental limitation of restricting their useable frequency bandwidth. The development of frequency-agile metamaterials has helped to alleviate these bandwidth restrictions by allowing real-time tuning of the metamaterial frequency response. We demonstrate electrically controlled persistent frequency tuning of a metamaterial, which allows the lasting modification of its response by using a transient stimulus. This work demonstrates a form of memory capacitance that interfaces metamaterials with a class of devices known collectively as memory devices.

The ability of metamaterials to create electromagnetic responses absent in nature has initiated the new research field of transformation optics (*1*, *2*), which has applications ranging from electromagnetic cloaking (*3*) to subdiffraction imaging (*4*). Frequency-agile metamaterials, which allow one to adjust the electromagnetic response in real time, are emerging as an important part of this field. The hybrid-metamaterial approach (*5*, *6*), in which natural materials are integrated into the metamaterial composite, has been particularly successful in enabling frequency-agile metamaterials that respond to the application of voltage (*7*, *8*), external electric field (*9*), light (*10*, *11*), and heat (*12*). This tuning ability helps make metamaterial devices more versatile, adapting to shifting input or changing target parameters. However, those methods for enabling frequency-agile metamaterials require the continuous application of an external stimulus to maintain altered metamaterial properties. Once the external stimulus is removed, the metamaterial returns to its original response. Essentially, any functionality derived from metamaterials would benefit greatly if the metamaterial tuning persisted once the triggering stimulus disappeared. Metamaterials that are tuned mechanically or geometrically should retain their tuned properties (*13*, *14*), but such techniques are likely to be difficult to implement at higher frequencies or for complex designs. We have achieved an electrically controlled memory effect using a hybrid device composed of a resonant metamaterial and a transition metal oxide. The principle underlying the persistent tuning of our hybrid device is that of memory-capacitance (memcapacitance for short), which was recently suggested theoretically (*15*).

The persistent frequency tuning of a memory metamaterial device can be illustrated by use of a single-layer gold split-ring resonator (SRR) array patterned (*16*) on a 90-nm-thin film of vanadium dioxide (VO_2) (Fig. 1A). VO_2 is a correlated electron material that exhibits an insulator-to-metal (IMT) phase transition that can be thermally (*17*), electrically (*9*, *18*), or optically (*19*) controlled. The IMT is percolative in nature and is initiated by the formation of nanoscale metallic puddles in the insulating host (*20*). The transition is highly hysteretic and has been previously shown to exhibit memory effects (*21*). The hysteresis associated with the VO_2 can be observed by measuring the dc resistance of the sample (Fig. 1B, solid lines). The phase transition also affects the dielectric properties of VO_2 in a specific way. At the onset of the IMT, electronic correlations acting in concert with the spatial inhomogeneity of VO_2 create a sharply divergent permittivity (*12*, *20*). This increasing VO_2 permittivity increases the capacitance of the SRR resonators so that the metamaterial resonance frequency decreases as the IMT progresses. The data in Fig. 1, B and C, illustrate this effect. At room temperature, we identify the resonance frequency of the SRR array as the spectral minimum at $\omega_0 = 1.65$ THz (Fig. 1C, darkest line). As the dielectric constant of VO_2 is increased with temperature, the resonance frequency red-shifts by as much as 20%. We show that this metamaterial resonance tuning persists when accomplished via short current pulses.

Because both the dc resistance and the permittivity are products of the IMT, the SRR resonance in the hybrid metamaterial inherits the same hysteretic nature observed in the dc resistance (*21*). Any transient excitation that causes a small perturbation in the VO_2 IMT will leave a lasting change of the resonance of the metamaterial. We can apply such an excitation voltage pulse using the electrical leads connected to the device. In this case, the applied voltage promotes the IMT by inducing local heating as current flows through the VO_2 film (*22*). In order to maximize the observable effect that small voltage pulses have on the metamaterial, we adjusted the temperature of the device to a range in which the hysteresis is most pronounced. This corresponds to a range in which the slope of the resistance as a function of temperature, $R(T)$, is the steepest,

[1]Department of Physics, University of California at San Diego (UCSD), La Jolla, CA 92093, USA. [2]Metal-Insulator Transition Lab, Electronics and Telecommunications Research Institute (ETRI), Daejeon 305-350, Republic of Korea. [3]School of Electrical and Engineering, Pukyong National University, Busan 608-739, Republic of Korea. [4]Center for Metamaterials and Integrated Plasmonics and Electrical and Computer Engineering Department, Duke University, Post Office Box 90291, Durham, NC 27708, USA.

*To whom correspondence should be addressed. E-mail: tdriscol@physics.ucsd.edu

and we chose 338.6 K (Fig. 1B, dashed line). Applying a series of voltage pulses (Fig. 2B) while spectroscopically monitoring the resonance frequency of our hybrid structure before and after each pulse (*12*), we were able to see the effect of these sequential voltage pulses (Fig. 2A). Each pulse consistently red-shifts the resonance frequency. This red shift is clearly visible even after the voltage is removed, demonstrating that a persistent change in the hybrid metamaterial was obtained. The volumetric heat capacity of the whole device is quite large given the rather limited power input with each pulse. Thus, this is not a global thermal effect; rather, heating is localized primarily to the VO_2 film and is transient. After the voltage pulse subsides, the device rapidly thermalizes back to the starting temperature. Temperature monitoring confirmed that the overall temperature was unchanged to within ±0.02 K during the entire duration of the experiment. The persistence of the modified resonance has been spectroscopically monitored for 10 min and did not show signs of degradation. Our work on the dc memory resistance of VO_2 suggests that the effect will persist much longer (*21*).

It is instructive to analyze the response of our device within an effective circuit model (*23*, *24*). Our SRR array can be modeled as an array of RLC circuit elements, each with resonance frequency $\omega = (LC)^{-1/2}$ (Fig. 2C). The inductance L is known to remain constant because no permeability changes occur in any material within our device. This allows us to relate changes of the observed resonant frequency directly to a variation in capacitance: $\frac{C}{C_0} = \left(\frac{\omega_0}{\omega}\right)^2$. We estimate the capacitance C_0 of a single SRR of our dimensions as $C_0 \approx 2.5 \times 10^{-15}$ Farad/SRR (*25*). The green points in Fig. 2A show the SRR capacitance in this manner. The plotted capacitance C is the total capacitance of each SRR. To model the persistent-tuning behavior of our device within the effective circuit picture, we introduced the circuit element of memory capacitance C_m (*15*), defined by the relations $q(t) = C_m(x,V_c,t)V_c(t)$ and $\dot{x} = f(x,V_c,t)$. V_c and $q(t)$ are the bias and charge, respectively, on the capacitor defined by VO_2, and x is a set of state variables that in the present case accounts for the dielectric behavior of the VO_2 IMT. C_m acts in parallel with the SRR natural capacitance to give a total capacitance of $C = C_0 + C_m$. In particular, C_m parameterizes the metamaterial-tuning memory effect demonstrated in Fig. 2A. The increasing conductivity of VO_2 as the IMT progresses also introduces a memory resistance (R_m) (Fig. 2B) [(*15*, *26*) and references therein]. R_m acts detrimentally to reduce the quality factor of the metamaterial resonance in our device. Thus, softening of the resonance that accompanies the reduced resonance frequency is apparent in the spectra (Fig. 1C). In VO_2, the memory resistance and memory capacitance appear to be inextricably intertwined, which is an effect that has also been anticipated theoretically and should be particularly relevant at the nanoscale (*15*). In our circuit model, V_{ext} is the applied voltage pulse that modifies C_m and R_m. V_{IR} originates from our infrared probe. Very different powers and time scales allow us to effectively separate the operation of the probing V_{IR} and modifying V_{ext} into the SRR- and VO_2-dominated groups (Fig. 2C). Specifically, the resonance frequency of the SRRs is much faster than the time scales of V_{ext}, and the power levels used for spectroscopic probing are much less than those necessary for the modification of C_m. Systems in which these conditions are not true will make interesting nonlinear study cases.

To better illustrate the operation of the device, we propose a thermal finite-element model (*16*) to examine the time-evolution of the VO_2 temperature for a range of input powers (Fig. 3A). The input power of the first four voltage pulses (α, β, γ, and δ) are marked, and for each a near steady-state rise in temperature (ΔT) quickly emerges. This thermal result enables a more detailed look at the evolution of capacitance during voltage pulses (Fig. 3B). Starting from data point A, with normalized capacitance $C = C_0$, the voltage pulse α raises the temperature of the VO_2 by $\Delta T_\alpha = 0.11$ K (as documented by the finite-element simulations), causing an increase in the capacitance. Once the voltage pulse stops, the VO_2 quickly (≲25 ms) (*16*) thermalizes back to the bias temperature of 338.6 K. However, because of the hysteresis in the IMT a net change in the capacitance persists, and the device settles to point B with capacitance $C = 1.006\ C_0$. These simulations reveal the complete heating/cooling cycle, which gives the switching time scale as set by the thermal geometry of the device close to ~50 ms. The arrows in Fig. 3B illustrate this hysteretic capacitance behavior by showing a probable path for $C(T)$ during this heating/cooling cycle between data points. These arrows were drawn by using the experimentally determined pre- and post- pulse capacitances from Fig. 2A, and the maximum temperature rise was revealed from simulations in Fig. 3A. This is coupled with an assumption that the hysteresis in the IMT is strong enough that the post-pulse thermalization cooling has little effect on the capacitance value. This latter assumption is well-supported by the much flatter slope observed in Fig. 1B for the dc resistance during cooling than heating at 338.6 K (dR_{heat}/dT = 100 kilohm per degree Kelvin and dR_{cool}/dT = 4 kilohm per degree Kelvin, where R_{heat} is the resistance during heating and R_{cool} is the resistance during cooling), as well as other work (*21*). However, with our current equipment configuration we are unable to experimentally probe the capacitance on time scales that are fast enough to directly obtain this

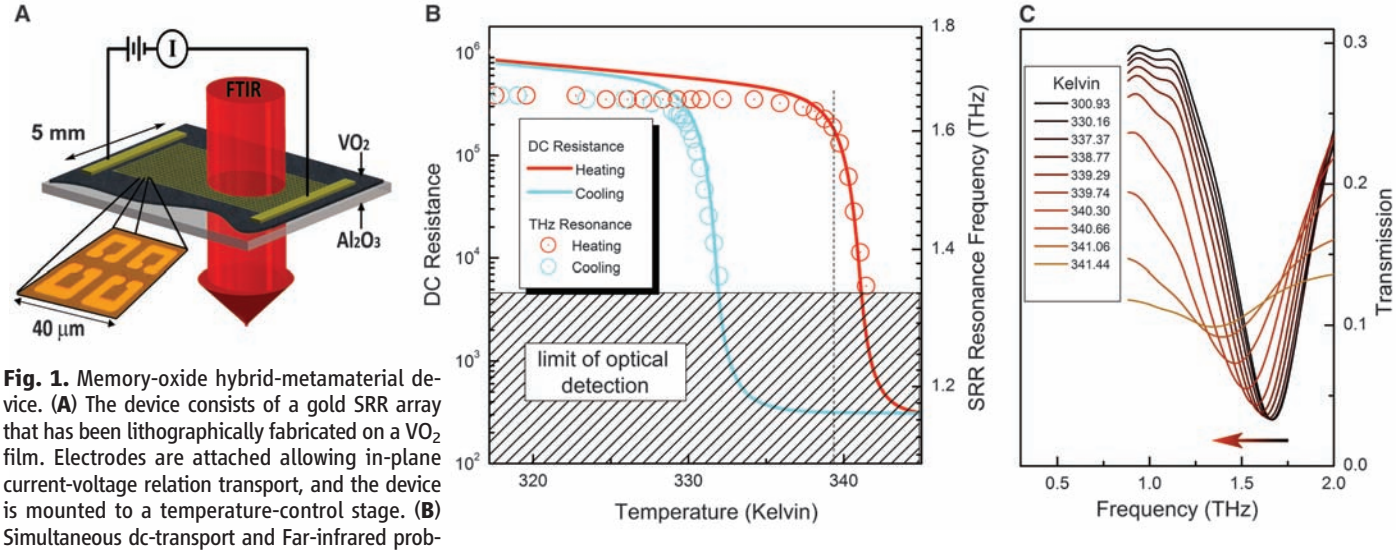

Fig. 1. Memory-oxide hybrid-metamaterial device. (**A**) The device consists of a gold SRR array that has been lithographically fabricated on a VO_2 film. Electrodes are attached allowing in-plane current-voltage relation transport, and the device is mounted to a temperature-control stage. (**B**) Simultaneous dc-transport and Far-infrared probing of the metamaterial demonstrate that as VO_2 passes through its insulator-to-metal transition, resistance drops and the SRR resonance frequency decreases. This latter effect occurs because of an increase in the per-SRR capacitance. (**C**) Spectroscopic data from which the metamaterial resonance frequencies in (B) are identified (heating cycle shown). Data in (B) and (C) were obtained by performing a complete temperature cycle (300 to 350 to 300 K) with the temperature stage on which the sample is mounted.

$C(T)$ data inside pulses. Nevertheless, it is clear that the demonstration of electrically controlled memory capacitance in this device relies on the hysteretic nature of the VO_2 phase transition.

We stress that the use of a temperature bias in our experiment is required only to put a particular VO_2 film into a regime in which the IMT is highly hysteretic, although our VO_2 does exhibit some hysteretic qualities even at room temperature (*16*). More promisingly, several VO_2 fabrication techniques are known to reduce the phase-transition temperature down to room temperature (*27*, *28*) and thus will enable VO_2-hybrid memory metamaterials to operate at ambient conditions. Additionally, any material that possesses a hysteretic response in either its permittivity or permeability at a suitable frequency range could be used in a hybrid-metamaterial design so as to obtain memory effects analogous to those we demonstrated here (*29*). The correlated electron state that gives VO_2 the divergent permittivity used in this demonstration is only effective up to mid-infrared. A combination of other hysteretic materials with metamaterials operational in the near-infrared and visi-

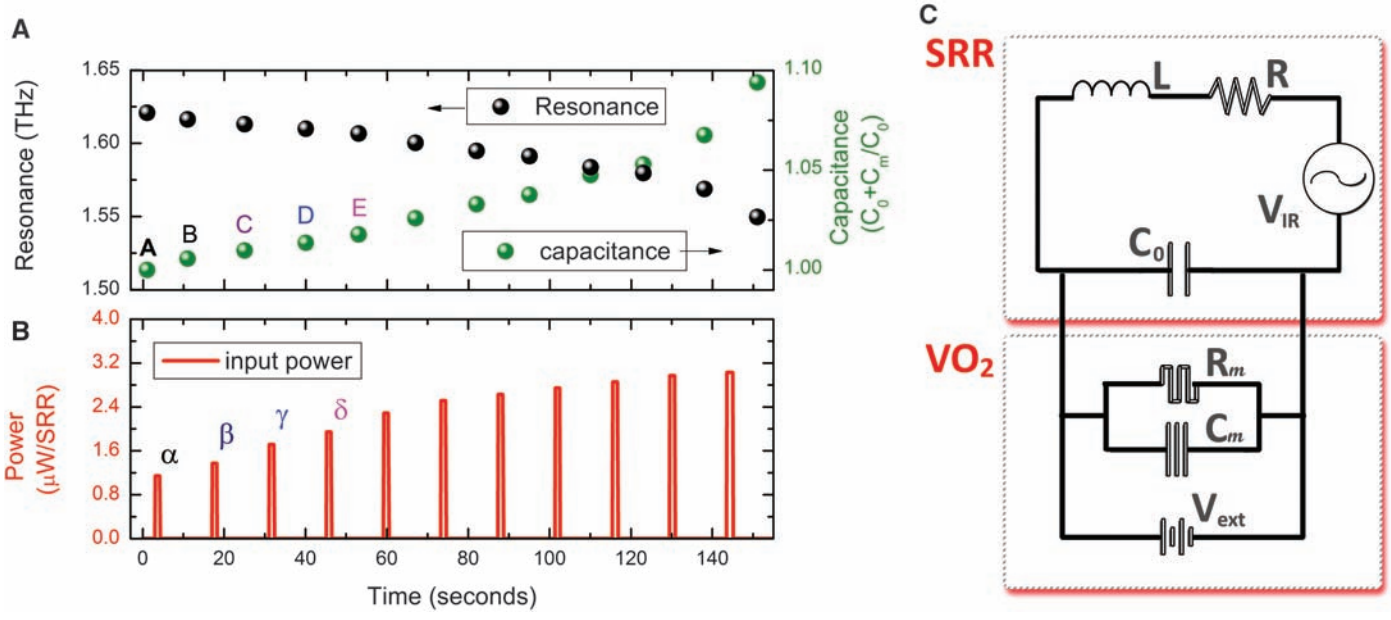

Fig. 2. Persistent electrical tuning of a metamaterial. (**A**) Successive modification of the resonance of the hybrid-metamaterial is achieved by sequential transient 1-s electrical pulses of increasing power. (**B**) These modifications persist until the device is thermally reset and have been measured to be stable over 20 min. This operation is well illustrated within the effective circuit model (**C**) by the addition of memory circuit elements $\mathbf{R_m}$ and $\mathbf{C_m}$ in parallel to the natural capacitance of the SRR.

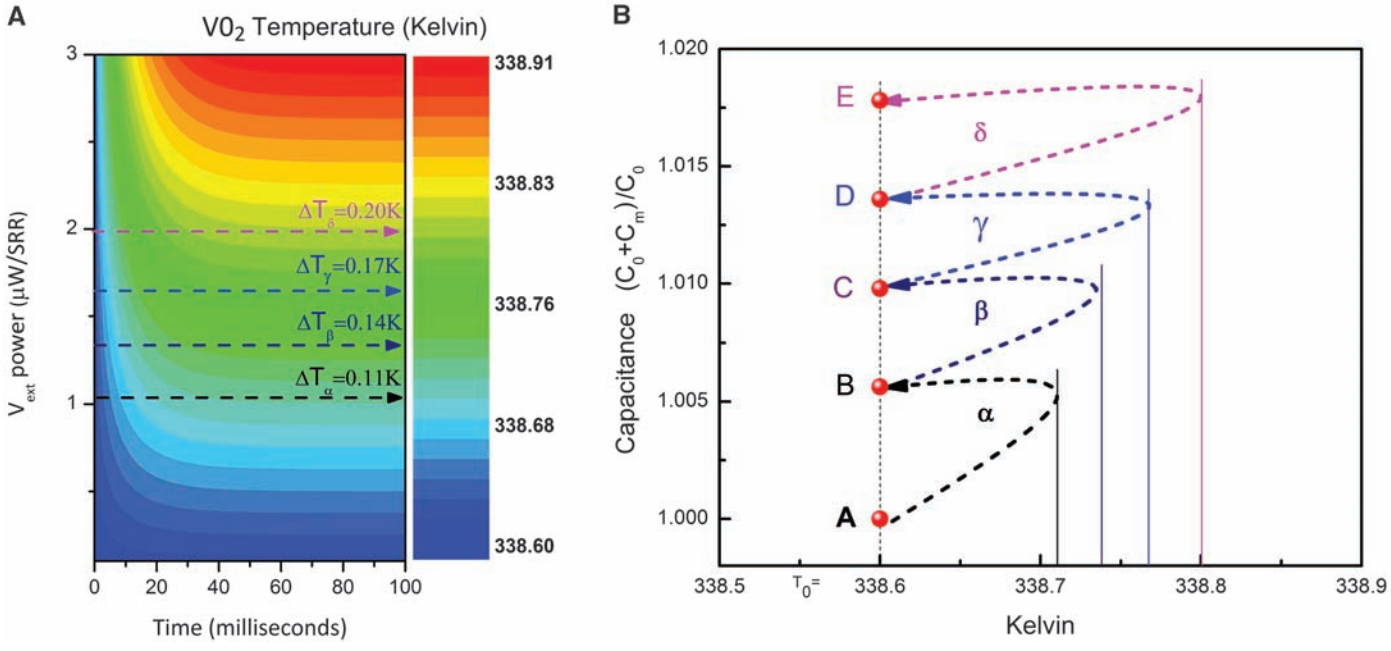

Fig. 3. The operation of memory capacitance explained via hysteretic phase transition. (**A**) Using a finite element model of our device, we calculated the temperature rise ΔT of the VO_2 film for a range of given input powers, including the first four voltage pulses in our experiment (α, β, γ, and δ). A steady-state temperature rise was observed to emerge quite quickly. (**B**) This temperature rise was used in combination with data from Fig. 2A to estimate and sketch the behavior of capacitance during heating and cooling.

ble spectra could easily push this effect to higher frequencies that are beneficial for a variety of practical applications (*30*).

References and Notes

1. D. Schurig, J. B. Pendry, D. R. Smith, *Opt. Express* **15**, 14772 (2007).
2. A. V. Kildishev, W. Cai, U. K. Chettiar, V. M. Shalaev, *N. J. Phys.* **10**, 115029 (2008).
3. J. B. Pendry, D. Schurig, D. R. Smith, *Science* **312**, 1780 (2006).
4. Z. Liu, H. Lee, Y. Xiong, C. Sun, X. Zhang, *Science* **315**, 1686 (2007).
5. H.-T. Chen *et al.*, *Appl. Phys. Lett.* **93**, 091117 (2008).
6. J. N. Gollub, J. Y. Chin, T. J. Cui, D. R. Smith, *Opt. Express* **17**, 2122 (2009).
7. H.-T. Chen *et al.*, *Nature Photon.* **2**, 295 (2008).
8. I. Gil *et al.*, *Electron. Lett.* **40**, 1347 (2004).
9. M. M. Qazilbash *et al.*, *Appl. Phys. Lett.* **92**, 241906 (2008).
10. W. J. Padilla, A. J. Taylor, C. Highstrete, L. Mark, R. D. Averitt, *Phys. Rev. Lett.* **96**, 107401 (2006).
11. A. Degiron, J. J. Mock, D. R. Smith, *Opt. Express* **15**, 1115 (2007).
12. T. Driscoll *et al.*, *Appl. Phys. Lett.* **93**, 024101 (2008).
13. I. V. Shadrivov, N. A. Zharova, A. A. Zharov, Y. S. Kivshar, *Phys. Rev. E Stat. Nonlin. Soft Matter Phys.* **70**, 046615 (2004).
14. T. Driscoll *et al.*, *Appl. Phys. Lett.* **91**, 062511 (2007).
15. M. Di Ventra, Y. V. Pershin, L. O. Chua, *Proc. IEEE* **97**, 1371 (2009).
16. Materials and methods are available as supporting material on *Science* Online.
17. A. Zylbersztejn, N. F. Mott, *Phys. Rev. B Solid State* **11**, 4383 (1975).
18. B.-G. Chae, H.-T. Kim, D.-H. Youn, K.-Y. Kang, *Physica B* **369**, 76 (2005).
19. S. Lysenko *et al.*, *Appl. Surf. Sci.* **252**, 5512 (2006).
20. M. M. Qazilbash *et al.*, *Science* **318**, 1750 (2007).
21. T. Driscoll, H. T. Kim, B. G. Chae, M. Di Ventra, D. N. Basov, *Appl. Phys. Lett.* **95**, 043503 (2009).
22. R. Lopez, L. A. Boatner, T. E. Haynes, R. F. Haglund Jr., L. C. Feldman, *Appl. Phys. Lett.* **85**, 1410 (2004).
23. G. V. Eleftheriades, O. Siddiqui, A. K. Iyer, *Microwave Wireless Compon. Lett. IEEE* **13**, 51 (2003).
24. J. D. Baena *et al.*, *Microwave Theory Tech. IEEE Trans.* **53**, 1451 (2005).
25. S. Tretyakov, http://arxiv.org/abs/cond-mat/0612247 (2006).
26. J. J. Yang *et al.*, *Nat. Nanotechnol.* **3**, 429 (2008).
27. Y. Muraoka, Z. Hiroi, *Appl. Phys. Lett.* **80**, 583 (2002).
28. H.-T. Kim *et al.*, *N. J. Phys.* **6**, 52 (2004).
29. I. Shadrivov, *SPIE Newsroom* doi:10.1117/2.1200811.1390 (2008).
30. V. M. Shalaev, *Nature Photon.* **1**, 41 (2007).

31. This work is supported by the U.S. Department of Energy (DOE), the Air Force Office of Scientific Research (AFOSR), and ETRI. Work at UCSD on VO_2 was supported by DOE–Basic Energy Sciences and the metamaterials work was supported by AFOSR and ETRI. M.D. acknowledges partial support from NSF. H.K. acknowledges research support from a project of the Ministry of Knowledge Economy in Korea.

Supporting Online Material

www.sciencemag.org/cgi/content/full/1176580/DC1
Materials and Methods
Fig. S1
Table S1
References

20 May 2008; accepted 4 August 2009
Published online 20 August 2009;
10.1126/science.1176580
Include this information when citing this paper.

Itinerant Ferromagnetism in a Fermi Gas of Ultracold Atoms

Gyu-Boong Jo,[1]* Ye-Ryoung Lee,[1] Jae-Hoon Choi,[1] Caleb A. Christensen,[1] Tony H. Kim,[1] Joseph H. Thywissen,[2] David E. Pritchard,[1] Wolfgang Ketterle[1]

Can a gas of spin-up and spin-down fermions become ferromagnetic because of repulsive interactions? We addressed this question, for which there is not yet a definitive theoretical answer, in an experiment with an ultracold two-component Fermi gas. The observation of nonmonotonic behavior of lifetime, kinetic energy, and size for increasing repulsive interactions provides strong evidence for a phase transition to a ferromagnetic state. Our observations imply that itinerant ferromagnetism of delocalized fermions is possible without lattice and band structure, and our data validate the most basic model for ferromagnetism introduced by Stoner.

Magnetism is a macroscopic phenomenon with its origin deeply rooted in quantum mechanics. In condensed-matter physics, there are two paradigms for magnetism: localized spins interacting via tunneling and delocalized spins interacting via an exchange energy. The latter gives rise to itinerant ferromagnetism, which is responsible for the properties of transition metals such as cobalt, iron, and nickel. Both kinds of magnetism involve strong correlations and/or strong interactions and are not yet completely understood. For localized spins, the interplay of magnetism with d-wave superfluidity and the properties of frustrated spin materials are topics of current research. For itinerant ferromagnetism (*1*–*7*), phase transition theories are still qualitative.

We implemented the Stoner model, a textbook Hamiltonian for itinerant ferromagnetism (*8*), by using a two-component gas of free fermions with short-range repulsive interactions, which can capture the essence of the screened Coulomb interaction in electron gases (*8*). However, there is no proof so far that this simple model for ferromagnetism is consistent when the strong interactions are treated beyond mean-field approaches. It is known that this model fails in one dimension, where the ground state is singlet for arbitrary interactions, or for two particles in any dimension (*3*). In our work, cold atoms were used to perform a quantum simulation of this model Hamiltonian in three dimensions, and we showed experimentally that this Hamiltonian leads to a ferromagnetic phase transition (*2*). This model was also realized in helium-3 (*9*), but the liquid turn into a solid phase and not into a ferromagnetic phase at high pressure. It has also been applied to neutrons in neutron stars (*10*).

To date, magnetism in ultracold gases has been studied only for spinor (*11*, *12*) and dipolar (*13*) Bose-Einstein condensates (BECs). In these cases, magnetism is driven by weak spin-dependent interactions, which nevertheless determine the structure of the condensate because of a bosonic enhancement factor. In contrast, here we describe the simulation of quantum magnetism in a strongly interacting Fermi gas.

An important recent development in cold atom science has been the realization of superfluidity and the BEC–Bardeen-Cooper-Schrieffer (BCS) crossover in strongly interacting, two-component Fermi gases near a Feshbach resonance (*14*). These phenomena occur for attractive interactions for negative scattering length and for bound molecules (corresponding to a positive scattering length for two unpaired atoms). Very little attention has been given to the region of atoms with strongly repulsive interactions. One reason is that this region is an excited branch, which is unstable against near-resonant three-body recombination into weakly bound molecules. Nevertheless, many theoretical papers have proposed a two-component Fermi gas near a Feshbach resonance as a model system for itinerant ferromagnetism (*15*–*22*), assuming that the decay into molecules can be sufficiently suppressed. Another open question is the possibility of a fundamental limit for repulsive interactions. Such a limit due to unitarity or many-body physics may be lower than the value required for the transition to a ferromagnetic state. We show that this is not the case and that there is a window of metastability where the onset of ferromagnetism can be observed.

A simple mean-field model captures many qualitative features of the expected phase transition but is not adequate for a quantitative description of the strongly interacting regime. The total energy of a two-component Fermi gas of average density n (per spin component) in a volume V is given by $E_F 2Vn\left\{\frac{3}{10}[(1+\eta)^{5/3}+(1-\eta)^{5/3}]+\frac{2}{3\pi}k_F a(1+\eta)(1-\eta)\right\}$, where E_F is the Fermi energy of a gas, k_F is the Fermi wave vector of a gas, a is the scattering length characterizing short-range interactions between the two components, and $\eta = \Delta n/n = (n_1 - n_2)/(n_1 + n_2)$ is the magnetization of the Fermi gas. The local magnetization of the Fermi gas is nonzero when the gas separates into two volumes, where the densities n_1 and n_2 of the two spin states differ

[1]Massachusetts Institute of Technology–Harvard Center for Ultracold Atoms, Research Laboratory of Electronics, Department of Physics, Massachusetts Institute of Technology, Cambridge, MA 02139, USA. [2]Department of Physics, University of Toronto, Toronto, Ontario M5S1A7, Canada.

*To whom correspondence should be addressed. E-mail: gyuboong@mit.edu